Review

Electrochemical Reduction of CO_2 Using Group VII Metal Catalysts

Jacob A. Barrett,[1] Christopher J. Miller,[1] and Clifford P. Kubiak[1,*]

Anthropogenic CO_2 emissions, primarily from the combustion of fossil fuels, are driving climate change at an alarming rate. Our current dependence on carbon-based fuels has motivated research interest in the capture and catalytic reduction of carbon dioxide back to liquid fuels. Electrochemical reduction of carbon dioxide has been intensely researched over the past decade. Here, some of the important contributions made to this field over the past decade using the Group VII transition metal bipyridine catalysts are reviewed. Strategies to further our mechanistic understanding of the electrocatalytic reduction of CO_2 to CO are described.

The Electrochemical Reduction of Carbon Dioxide

The reduction of carbon dioxide back to energy-rich fuels has challenged chemists for over 100 years, with the first reports appearing in the early 1900s [1,2]. Today, the field of **solar fuels** (see Glossary) seeks to store renewable solar energy as chemical energy by the electrochemical or photoelectrochemical reduction of CO_2 [3,4]. In recent years, the state of California has had surpluses of electricity due to the large quantities of solar electricity coming onto the electrical power grid in the middle of the day [5]. Liquid solar fuels are attractive alternatives to batteries as a means of storage of renewable energy for later use [4,6,7]. The first molecular catalysts for the **electrochemical reduction** of CO_2 were reported in the 1960s and 1970s. These were transition metal **electrocatalysts** [8,9] based on metal phthalocyanine complexes [10,11], metal tetraaza-macrocycles [12,13], late metal phosphine complexes [14], and Re (I) bipyridyl carbonyl complexes [15]. In this brief review, we present the current status of the field and its future.

A molecular electrocatalyst both participates in an electron transfer reaction (at an electrode) and accelerates the rate of a chemical reaction. An electrocatalyst both supplies charge and performs inner sphere chemical reduction or oxidation of an otherwise kinetically stable substrate. Thus, both the electron transfer and the chemical kinetics must be fast for an electrocatalyst to be efficient. Ideally, the redox potential (E_0) of the electrocatalyst electron transfer reaction should thermodynamically match the chemical potential difference between products and reactants (i.e., the free energy of the reaction) of the catalyzed process (e.g., reduction of CO_2) [16]. A significant advantage of molecular electrocatalysis is that these factors can be optimized by appropriate ligand design, choice of metal, and d-electron configuration. New dimensions in the optimization of molecular catalysts have also been identified. In the past decade, breakthroughs in our understanding of how molecular catalysts respond to their local environment, such as solvent, electrolyte, cofactors, and applied bias, have given researchers new tuning strategies. Herein, the knowledge that has been gained recently on the electrochemical reduction of CO_2 by molecular catalysts is presented and key methods are identified where research has continued to expand our understanding and control of the CO_2 reduction reaction.

This brief review focuses on the production of CO from CO_2 using Group VII (Mn and Re) metal catalysts. There is a plethora of important research on the production of formate [17–21] from

Highlights

Extensive spectroscopic studies of molecular electrocatalysts have enabled several design approaches for the creation of new functional electrolysis systems for carbon dioxide reduction.

Reaction pathways can be manipulated by controlling a number of factors affecting the chemical environment through careful selection of Lewis or Brønsted acids or synthetic modification that controls metal–metal interactions, including noncovalent interactions like hydrogen bonding.

IR spectroelectrochemistry has proved to be a valuable tool for observing chemical characteristics of electrocatalysts at catalytically relevant potentials and understanding the intermediates between the catalyst precursor and active catalyst states.

[1]Department of Chemistry and Biochemistry, University of California, San Diego, 9500 Gilman Drive, La Jolla, CA 92093-0358, USA

*Correspondence:
ckubiak@ucsd.edu (C.P. Kubiak).

CO$_2$ as well as formaldehyde [22], methanol [23], and multicarbon products [24], which are not discussed in this review. The focus of this review is recent research on the reaction mechanisms and current understanding of how immobilization on the electrode surface alters Mn and Re bipyridyl carbonyl catalysts.

Group VII Metal Bipyridine Electrocatalysts

Lehn and coworkers discovered that Re(bpy)(CO)$_3$Cl catalyzes electrochemical CO$_2$ reduction [15]. Lehn reported that, under inert conditions, Re(bpy)(CO)$_3$Cl showed a reversible one-electron reduction followed by a second, irreversible one-electron reduction. Under an atmosphere of CO$_2$, there is a large current increase following the second reduction, indicative of CO$_2$ reduction catalysis. This system reduced CO$_2$ to CO at −1.49 V vs saturated calomel electrode (SCE) (ca −1.9 V vs Fc$^{+/0}$) in 9:1 N,N-dimethylformamide (DMF)/H$_2$O with a very high **Faradaic efficiency (FE)** for CO over H$_2$ evolution (FE$_{CO}$ = 98%). However, the rate of catalysis, defined by the **turnover frequency (TOF)**, was reported to be relatively slow (TOF = 21.4 h^{-1}). The catalyst operates best at a 1.0 V **overpotential** (relative to the standard potential for protic CO$_2$ reduction) [16,25,26]. Furthermore, 100% CO selectivity is observed in wet MeCN or DMF or with a weak acid present such as trifluoroethanol (TFE) or phenol (PhOH). By optimization of reaction conditions, a maximum TOF greater than 500 s^{-1} could be achieved with greater than 10^7 turnover number (TON) (Figure 1).

Mechanistic Studies of Re Bipyridine Catalysts

In 2010, Kubiak and coworkers initiated studies of the Re(bpy)(CO)$_3$Cl catalyst focused on mechanistic understanding and identification of design principles that could be used to develop new
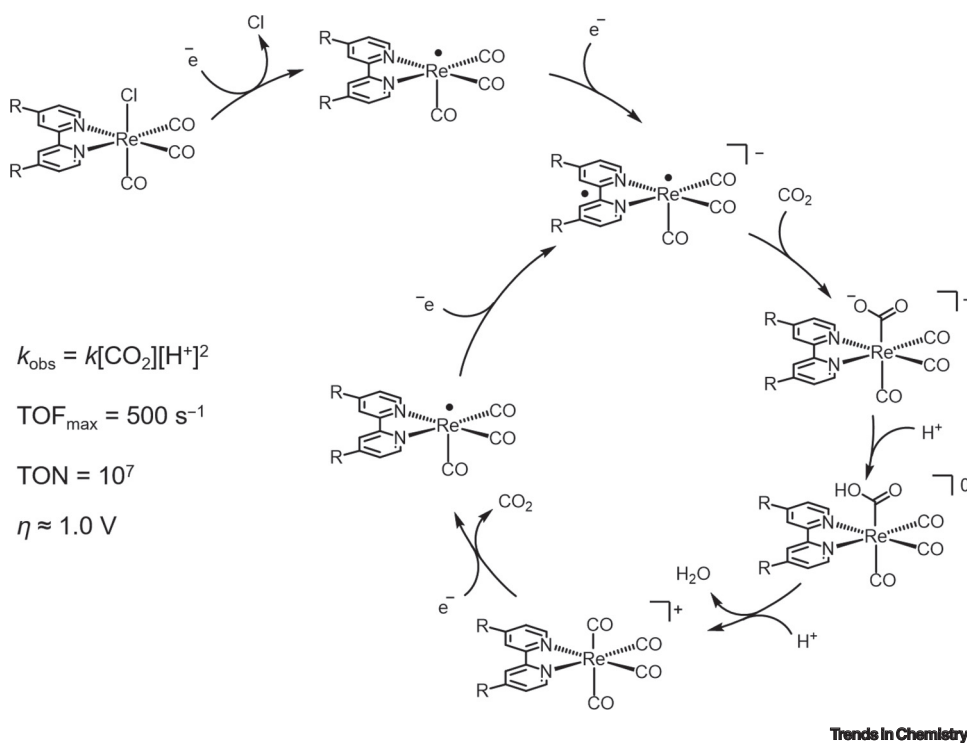

$k_{obs} = k[CO_2][H^+]^2$

$TOF_{max} = 500 \text{ s}^{-1}$

$TON = 10^7$

$\eta \approx 1.0 \text{ V}$

Trends in Chemistry

Figure 1. Proposed Mechanism for the Electrocatalytic Reduction of CO$_2$ by Re(bpy)(CO)$_3$Cl [27]. See also [25,28–30]. Abbreviations: TOF, turnover frequency; TON, turnover number.

Glossary

Cyclic voltammetry (CV): a typical experiment uses a reference electrode (a standard potential), a working electrode (where the potential is applied), and a counter electrode (closes the current circuit). This electrochemical technique measures the current in the electrochemical cell as a function of the applied potential at the working electrode.

d_z^2 orbital: refers to the atomic orbital that occupies the z-axis of an metal atom.

Electrocatalyst: a molecule that can change and increase the rate of an electrochemical reaction without being consumed in the reaction.

Electrochemical reduction: a chemical reaction involving the transfer of electrons from the electrode to the surface.

Faradaic efficiency (FE): the percentage of the charge transferred in a system that facilitates a specific reaction.

Hammett parameter: a linear free-energy relationship for modeling the electronic effect of substituents on aromatic systems.

IR spectroelectrochemistry (IR-SEC): IR spectroscopy of a specially designed electrochemical cell, which provides qualitative and quantitative information on the processes occurring under applied potential.

Overpotential: the potential difference between the standard potential and the potential where the redox event is observed, or the 'extra' potential needed to drive a redox reaction.

Solar fuel: a fuel synthesized from small ubiquitous molecules (i.e., water, carbon dioxide, nitrogen) using solar energy.

Stopped flow: a technique for observing chemical reaction kinetics on the millisecond timescale.

Sum-frequency generation (SFG): a nonlinear spectroscopic technique used to analyze surfaces. This typically involves two laser incident sources, which generate an output that is the sum of the two incident light sources.

Tafel plot: a plot of the Tafel equation, which relates the rate of an electrochemical reaction to the overpotential applied to achieve that rate.

Turnover frequency (TOF): a measure of the rate of a catalyst and calculated as the number of chemical conversions of a substrate per second facilitated by the catalyst. This is related to the TON,

and better catalysts [31]. **IR spectroelectrochemistry (SEC)** studies and independent syntheses of the reduced states indicated that significant Re(0)–Re(0) dimer formation occurs after the first reduction [32]. The second reduction is required to break the Re–Re bond to produce the proposed active catalyst, [Re(bpy)(CO)$_3$]$^-$. To inhibit dimer formation, *tert*-butyl groups were added to the 4,4' positions of the bipyridine ligand of the catalyst [Re(*t*Bu-bpy)(CO)$_3$Cl] [31]. IR-SEC indicated significant inhibition of dimer formation with the *tert*-butyl bpy complex. The IR-SEC studies were also important in establishing intermediates that are formed in the reduction of Re(*t*Bu-bpy)(CO)$_3$Cl to the active catalyst, [Re(*t*Bu-bpy)(CO)$_3$]$^-$. These studies revealed that the first reduction is bpy ligand based, but this species is unstable with respect to halide ligand dissociation and electron migration to the rhenium center to afford the radical •Re(*t*Bu-bpy)(CO)$_3$. Following the second reduction, the anion [Re(*t*Bu-bpy)(CO)$_3$]$^-$ has two ν(CO) bands observed at 1940 and 1832 cm^{-1} (Figure 2). Density functional theory (DFT) [29] and Raman [33] and X-ray absorption spectroscopy [29] of this species indicate that the first reduction is ligand based, followed by a reduction at the metal center to produce the catalytically active species, which is best described as [Re(0)(*t*Bu-bpy•)(CO)$_3$] where one electron is localized to the Re **d_z^2 orbital** and the second to the bpy π^* orbital.

The rate of catalytic reduction of CO$_2$ by Re(*t*Bu-bpy)(CO)$_3$Cl exhibits a first-order kinetic dependence on [CO$_2$]. Mechanistic studies used IR **stopped-flow** experiments to examine the [CO$_2$] dependent reaction of [Re(*t*Bu-bpy)(CO)$_3$]$^-$ with CO$_2$ (Figure 2) [34]. The lowest energy ν(CO) band at 1832 cm^{-1} decays with a first-order dependence on [CO$_2$] leading to a new band at 1940 cm^{-1} even in the absence of Brønsted acid, where the solvent acts as the proton source [25]. Thus, on the timescale of seconds, the reaction with CO$_2$ is essentially a two-electron oxidative addition. The Re(I) complex produced by the reaction with CO$_2$ corresponded to Re(COOH) (*t*Bu-bpy)(CO)$_3$. We have come to call such species 'hydroxycarbonyls' rather than the frequently used term 'metallo-carboxylic acid'. The reason for this is that the species is a much better OH$^-$
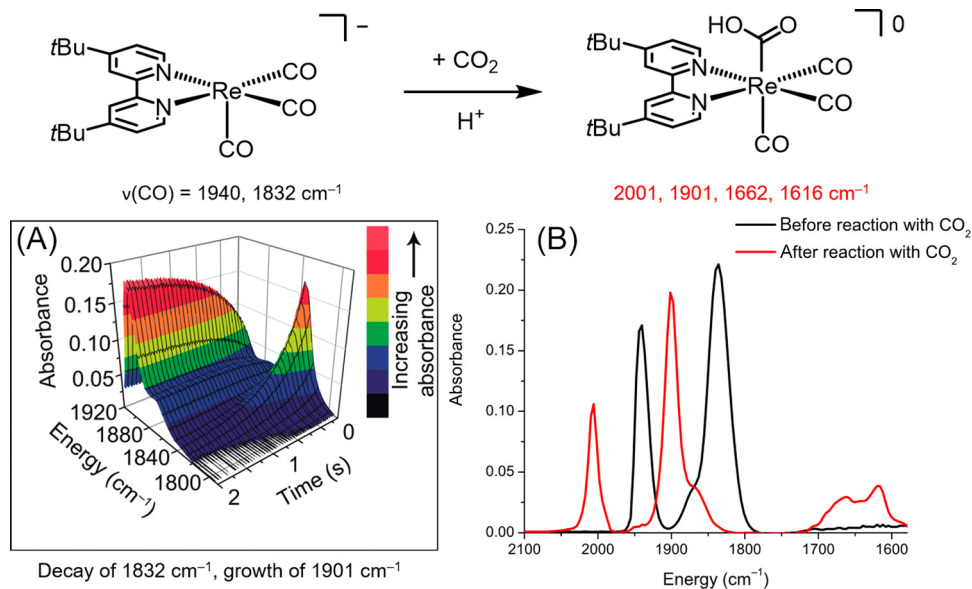
Figure 2. Proposed Mechanism for CO$_2$ Binding for [Re(*t*Bu-bpy)(CO)$_3$]$^-$ and IR Stretching Frequencies Associated with the Reduced Anion (Black) and Hydroxycarbonyl (Red). (A) 3D plot of IR spectra for 2.5-mM Re (*t*Bu-bpy)(CO)$_3$Cl with 32-mM CO$_2$ in tetrahydrofuran (THF). (B) IR spectra before (black) and after (red) reaction with CO$_2$ [27]. See also [25,29,34].

donor than acid. It readily combines with a second proton to produce $[Re(tBu\text{-}bpy)(CO)_4]^+$ and H_2O. The intermediate, $[Re(COO)(tBu\text{-}bpy)(CO)_3]^-$, is not observed. Reduction of $[Re(tBu\text{-}bpy)(CO)_4]^+$ regenerates the active catalyst $[Re(R\text{-}bpy)(CO)_3]^-$, liberating CO. Independent synthesis of the Re(I) tetracarbonyl species $[Re(bpy)(CO)_4](OTf)$ and $[Re(tBu\text{-}bpy)(CO)_4](OTf)$ determined that their reduction potentials were almost 500 mV more positive than the catalytic operating potential, implying that CO elimination and catalyst regeneration is not rate limiting [25,35]. The single electron reduction of these d^6 Re(I) complexes produce formally 19-electron intermediates, which greatly labilize the CO ligands. Combining these studies, a mechanism (shown in Figure 1) was proposed for CO_2 reduction with the $Re(R\text{-}bpy)(CO)_3X$ catalysts (R = tBu, H, or CH_3; X = halide, solvent). DFT calculations on the Re-centered radical $\bullet Re(bpy)(CO)_3$ indicated that the insertion of CO_2 into a Re carboxylate dimer $[Re(Me\text{-}bpy)(CO)_3]_2(\mu\text{-}CO_2)]$ provides another possible pathway for CO_2 reduction by a proton-independent process that produces CO and CO_3^{2-} [25]. This proposed mechanism was also supported by DFT calculations from Agarwal, Schaefer, and coworkers [36].

In the stopped-flow experiments with $[Re(tBu\text{-}bpy)(CO)_3]^-$, the kinetic selectivity for CO_2 reduction over H^+ reduction was greater than 50:1 when MeOH was used as the H donor. The reduced species $[Re(tBu\text{-}bpy)(CO)_3]^-$ reacts with CO_2 approximately ten times faster than $[Re(bpy)(CO)_3]^-$, suggesting an additional effect of the electron-donating tBu substituents. A DFT theoretical investigation suggests that the high selectivity for CO_2 reduction over H_2 evolution is due to the mixed metal–ligand character of the ground state of $[Re(R\text{-}bpy)(CO)_3]^-$ [29]. The formation of a metal hydride requires the electron density to be localized in the d_z^2 orbital. It is suggested that the 'non-innocent' ground state enables reaction with CO_2 through σ and π interactions with a lower reorganization energy near the transition state. Thus, CO_2 reduction is kinetically favored over H_2 evolution [29]. The DFT study indicates that the formation of the hydroxycarbonyl complex has a lower activation energy than protonation of $[Re(bpy)(CO)_3]^-$ to produce the Re–hydride, although the hydride is thermodynamically more stable (Figure 3) [26].

The overpotential and CO_2/H^+ selectivity are affected by the acid used. The lower the pK_a of the acid, the higher the catalytic current and the lower FE for CO_2 reduction with $Re(tBu\text{-}bpy)(CO)_3Cl$. This was observed using a range of acids like acetic acid ($pK_a = 23.5$ in MeCN), phenol ($pK_a = 29.1$ in MeCN), and TFE ($pK_a = 35.4$ in MeCN). The presence of a proton donor helps to achieve the stable intermediate $Re(COOH)(bpy)(CO)_3$; however, stronger proton donors result in increased H_2 reduction.

Mechanistic Studies of Mn Bipyridine Catalysts

Manganese bipyridine catalysts have been studied as more Earth-abundant and less expensive alternative CO_2 reduction catalysts compared with the $Re(R\text{-}bpy)(CO)_3X$ catalysts [37–45]. Originally reported as unreactive towards CO_2 [35], $Mn(R\text{-}bpy)(CO)_3X$ compounds were later found by Bourrez, Deronzier, and colleagues to show two one-electron reductions in their cyclic voltammograms and to catalytically reduce CO_2 provided significant quantities of water are present. Electrocatalysis occurs at the second reduction and at lower overpotentials (~400 mV) than $Re(R\text{-}bpy)(CO)_3X$ [37]. On closer examination, it was learned that the $Mn(R\text{-}bpy)(CO)_3X$ compounds have important and interesting mechanistic differences from their Re counterparts.

IR-SEC of $Mn(tBu\text{-}bpy)(CO)_3Br$ indicates that the first reduction is metal based and subsequent bromide loss results in a five-coordinate Mn-centered radical [46]. This quickly dimerizes to form $[Mn(tBu\text{-}bpy)(CO)_3]_2$. The dimerization rate is 10^9 times faster than the Re analog [26,47,48]. The doubly reduced species $[Mn(tBu\text{-}bpy)(CO)_3]^-$ is formed {analogous to $[Re(bpy)(CO)_3]^-$} after reductive cleavage of the dimer, observed after the second reduction wave in **cyclic voltammetry (CV)** [37,47,49].
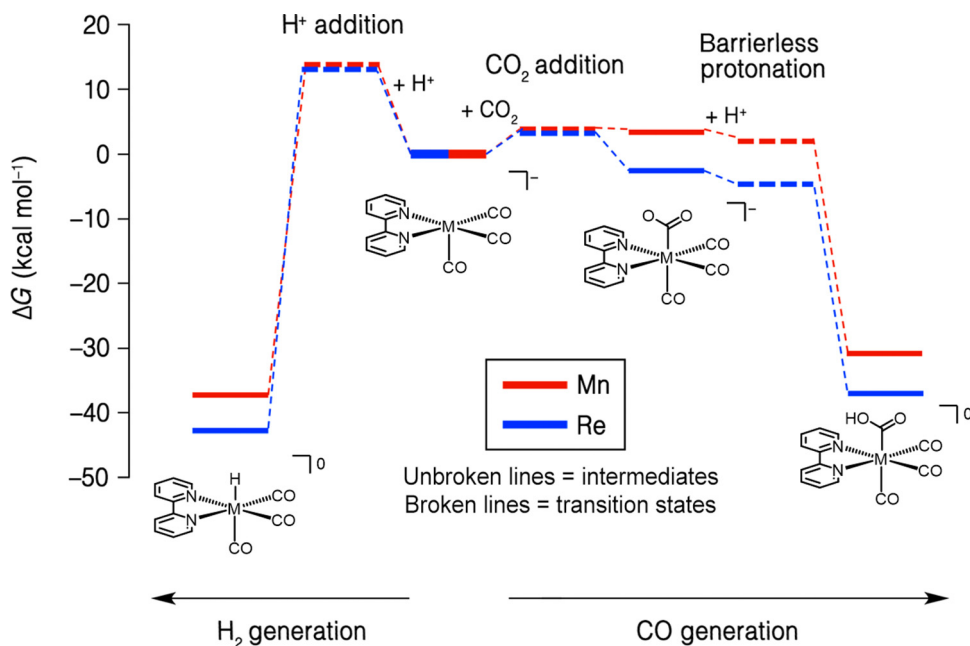
Figure 3. Potential-Energy Surface for H$^+$ or CO$_2$ Addition to Active Group VII Catalysts [26]. See also [25].

The formation of Mn^0–Mn^0 dimers is hindered by the use of bulky bipyridine ligands [50]. This strategy was used to bypass the dimerization/high-potential dimer reduction steps. In general, a radical has a less-negative reduction potential than a dimer of two of those radicals united by a covalent bond. Thus, Mn(mes-bpy)(CO)$_3$Br (where mes-bpy = 6,6'-dimesityl-2,2'-bipyridine) is reduced via a single two-electron process (Figure 4) to form the catalytically active species [Mn(mes-bpy)(CO)$_3$]$^-$. IR-SEC and chemical reductions with KC$_8$ further confirmed the formation of both the singly reduced and the doubly reduced Mn complexes at the same potential. This reduction potential (–1.55 V vs Fc$^{+/0}$) is hundreds of millivolts lower than other Mn(R-bpy)(CO)$_3$Br complexes, resulting in a lowering of the overpotential. CO$_2$ binding occurs at the reversible reduction potential with modest current after –1.6 V vs Fc$^{+/0}$. However, at more-negative potential (–2.0 V vs Fc$^{+/0}$), an unexpected and quite spectacular 'super-catalysis' (TOF = 5000 s^{-1}) occurs where there are no known redox processes for the catalyst. IR-SEC under CO$_2$ with a Brønsted acid reveals two potential-dependent catalytic pathways. The super-catalysis pathway occurs by reduction of the Mn(I) hydroxycarbonyl intermediate [Mn(COOH)(R-bpy)(CO)$_3$], which is formed in the electrochemical two-electron reduction at –1.55 V vs Fc$^{+/0}$ followed by protonation to form CO and water. The 'slow-catalysis' pathway occurs by protonation of the hydroxycarbonyl intermediate, which produces [Mn(mes-bpy)(CO)$_4$]$^{1+}$ and water, followed then by reduction.

An alternative proposal that was raised was that the Mn–Mn dimer and not the anionic species was the active catalyst. The Mn^0–Mn^0 dimer photochemically and electrochemically reduces CO$_2$ to formic acid or CO at a much slower rate than electrocatalytic CO$_2$ reduction to CO by [Mn(R-bpy)(CO)$_3$]$^-$ [26,47,48]. The electrocatalytic reaction was experimentally determined to follow kinetics that are first-order in catalyst, suggesting that the catalytic intermediate should be a mononuclear single-site catalyst and not dimeric [26,51,52].

In general, most of the Group VII CO$_2$ reduction electrocatalysts show kinetics where the rate-limiting step is C–O bond cleavage [50,53]. This has drawn attention to the question of how to
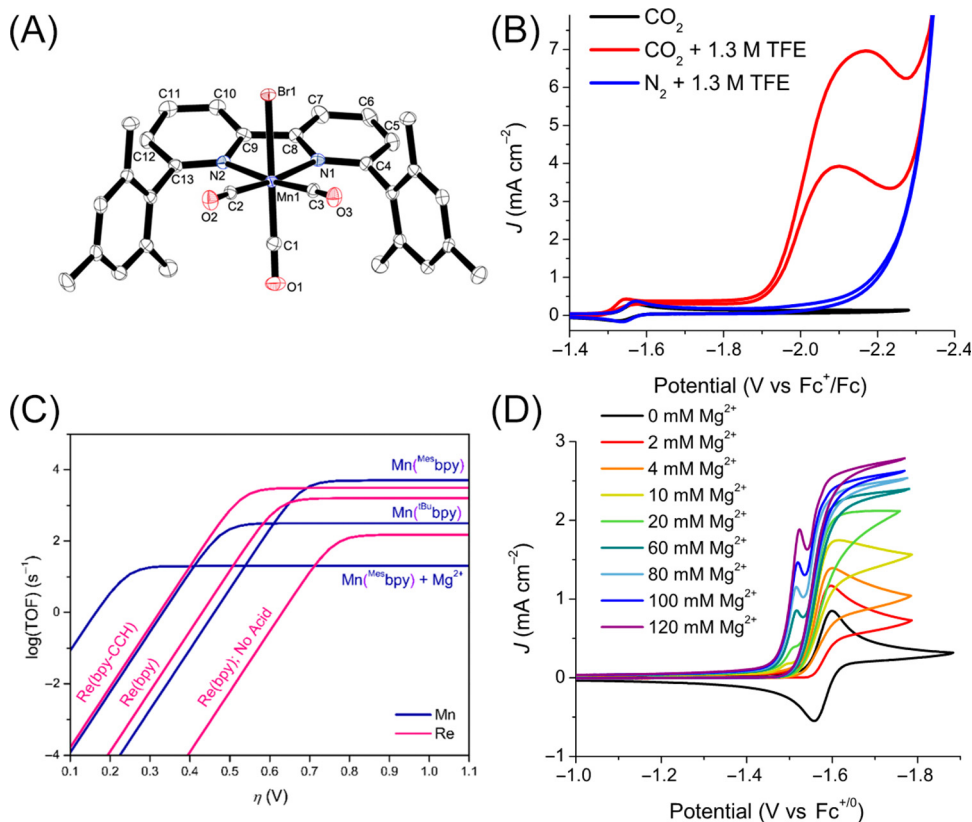
Figure 4. Mechanistic Studies of Mn Bipyridine Catalysts. Top left: Molecular structure of Mn(mes-bpy)$(CO)_3$Br with ellipsoids shown at 50% probability level [51]. Top right: Cyclic voltammetry (CV) of 1-mM Mn(mes-bpy)$(CO)_3$Br in 0.1-M TBAPF$_6$/MeCN using a glassy carbon electrode (GCE) with a scan rate of 0.1 V/s. Bottom left: Catalytic Tafel plot showing the relation of the catalytic rate to the overpotential for various Mn and Re catalysts in 0.1-M Bu$_4$NPF$_6$/MeCN with added Brønsted acid. Re(bpy-CCH) and Re(bpy) with 1.5-M trifluoroethanol (TFE). Mn(*t*Bu-bpy) with 1.4-M TFE. Mn(mes-bpy) with 0.3-M TFE. Bottom right: CV of [Mn(mes-bpy)$(CO)_3$(MeCN)]$^+$ under CO_2 in 0.1-M Bu$_4$NPF$_6$/MeCN with the addition of Mg^{2+} [50]. Abbreviation: TOF, turnover frequency.

facilitate C–O bond breaking of the bound CO_2 molecule to enhance the catalytic rate at low overpotential. Two promising strategies are use of strong Brønsted acids [54] or Lewis acids [55]. Lewis acids were shown to accelerate the rate of the Mn(mes-bpy)$(CO)_3$Br 'slow' process [50]. The addition Mg(OTf) increased the catalytic rate tenfold at 300 mV overpotential, one of the lowest observed overpotentials for homogeneous CO_2 reduction (Figure 4). CV indicated that the reaction is first order in Mg^{2+} and electrocatalyst, but second order in CO_2. In the proposed mechanism after CO_2 binds to the reduced catalyst, [Mn(mes-bpy)$(CO)_3$]$^-$, Mg^{2+} and a second equivalent of CO_2 undergo a condensation to form a Mg(C_2O_4) intermediate, which disproportionates to CO and MgCO$_3$. After the complex releases MgCO$_3$, [Mn(mes-bpy)$(CO)_4$]$^{1+}$ is formed. Two-electron reduction of the tetracarbonyl species regenerates the catalytically active species [Mn(mes-bpy)$(CO)_3$]$^-$ and releases CO. IR-SEC indicates carbonate/bicarbonate formation at potentials more negative than −1.4 V vs SCE (*ca* −1.8 V vs Fc$^{+/0}$) when a new, intense band appears at 1650 cm^{-1}. Magnesium carbonate, MgCO$_3$, is insoluble in MeCN and precipitates onto the electrode, hindering activity. However, chelated Lewis acids were shown to circumvent this solubility issue. [Zn(cyclam)]$^{2+}$ can be used to improve the electrochemical reduction of CO_2 by Mn(mes-bpy)$(CO)_3$Br [56].

Group VI Metal Bipyridine Electrocatalysts

The Kubiak and Cowan groups have examined electrocatalytic CO_2 reduction with bipyridine complexes of Group VI metals. The metal tetracarbonyl bipyridyl complexes $M(R\text{-bpy})(CO)_4$ (M = Mo, W; R = H, tBu) are active for CO_2 reduction with quantitative FE for CO at -2.3 V vs SCE (ca -2.7 V vs $Fc^{+/0}$) in MeCN [57]. DFT calculations revealed stronger π-back bonding into the CO ligands with Group VI metals compared with Re, suggesting that CO release from $[M(R\text{-bpy})(CO)_4]^{2-}$ limits the CO_2 reduction rates of these complexes. The catalytic onset potential of $[M(\text{bpy})(CO)_4]$ (M = Mo, W, Cr) was anodically shifted at Au electrodes compared with glassy carbon (GC) electrodes [58]. Cowan and coworkers used vibrational **sum-frequency generation (SFG)** spectroscopy to show that CO loss is enabled by strong interactions with the Au surface, providing access to a lower-energy pathway for generation of the active species $[M(\text{bpy})(CO)_3]^{2-}$ [59]. This is an example of chemically relevant surface interactions that the electrode materials may have in otherwise 'homogeneous' molecular electrocatalysis.

Immobilized Molecular Catalysts

Heterogeneous catalysts are typically the least selective and are mechanistically challenging to study. While in practice, the most important step in a catalytic process for fine chemical production, like pharmaceuticals, is selectivity, solid-phase catalysts are often used in industrial processes due to high stability, activity, lower loadings of active catalyst, ease of separation of products, and facile scalability. However, highly selective heterogeneous catalyst discovery is hindered by a lack of mechanistic understanding and thus often relies on high-throughput screening [60]. By contrast, molecular catalysts are among the most selective and mechanistically well understood catalysts. Immobilizing molecular catalysts onto surfaces allows direct control and the study of heterogeneous active sites, providing mechanistic insight on surface processes. One example of this is the Group VII electrocatalysts, as they are sufficiently understood with regard to their homogeneous reaction mechanisms and have thus been used to enable and understand the mechanisms at an electrode surface that produce a highly selective CO_2 reduction system and provide insight that is unattainable for heterogeneous catalysts presently.

Covalent and noncovalent surface attachment strategies can produce functional heterogenized molecular catalysts [61–64]. Immobilization techniques have ranged from polymer films [65,66] to Au–S self-assembled monolayers, electrografting to form new bonds [67], and adsorption to graphitic surfaces [68,69]. While the success of CO_2 reduction and stability vary for these systems, they have provided new insights on the chemistry at electrode surfaces.

Alkyne and alkene modified $Re(\text{bpy})(CO)_3Cl$ catalysts have been attached to a carbon electrode via polymer films [70–72]. While these systems were able to reduce CO_2 to CO, the long-term stability was affected by catalyst degradation and highlighted the need for more controlled immobilization techniques. The Marinescu group used a (2,2′-bipyridine)-5,5′-bis(diazonium) rhenium complex to make conjugated polymers attached to electrode surfaces [73]. These systems were able to reduce CO_2 to CO at a FE of 99% at -2.25 V vs $Fc^{+/0}$ (Figure 5). To bypass polymer films, $Re(t\text{Bu-bpy})(CO)_3Cl$ was physically adsorbed onto multiwall carbon nanotubes (MWCNTs) and was found to be highly active for CO_2 reduction under aqueous conditions (0.5 M $KHCO_3$). Controlled-potential electrolysis at -0.56 V vs reversible hydrogen electrode (RHE) (-1.2 V vs Ag/AgCl) showed these electrodes produced CO from CO_2 with 99% selectivity over 7 h and maintained a consistent current density over 60 min (Figure 5). The observed catalytic current density increased with more catalyst, up to 23.1 wt% Re; however, at 25.2 wt% Re in the composite material, current density decreased. This result suggests that the bulk of the material loaded into the MWCNTs is not participating in electrocatalysis.
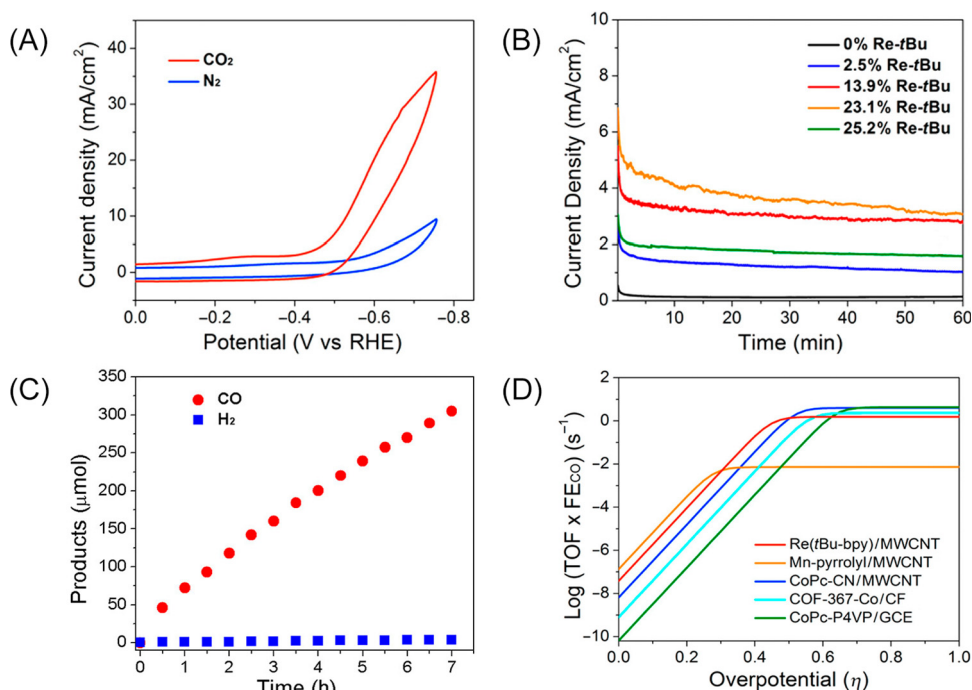
Figure 5. Mechanistic Studies of Immobilized Molecular Catalysts. Top left: Cyclic voltammetry (CV) of Re(tBu-bpy)(CO)$_3$Cl/multiwall carbon nanotube (MWCNT)/carbon nanofiber (CNF) electrode under N$_2$ (blue) and CO$_2$ (red) in 0.5-M KHCO$_3$ [75]. Re(tBu-bpy)/MWCNT is the working electrode, Ag/AgCl is the reference, and Pt is the counter electrode. Scan rate 100 mV/s. Top right: Controlled potential electrolysis with the electrodes in CO$_2$-saturated 0.5-M KHCO$_3$ at −0.58 V vs reversible hydrogen electrode (RHE). Bottom left: CO$_2$ and H$_2$ production over time. Bottom right: Catalytic Tafel plot comparing Re(tBu-bpy)(CO)$_3$Cl/MWCNT with other CO$_2$ reduction catalysts (Mn-pyrrolyl = {Mn[4,4′-di(1H-pyrrolyl-3-propyl carbonate)-2,2′-bipyridine](CO)$_3$MeCN}$^+$(PF$_6$)$^-$, CoPc-CN = cobalt-2,3,7,8,12,13,17,18-octacyanophthalocyanine, COF-367-Co = cobalt porphyrin in biphenyl-4,4′-dicarboxaldehyde covalent organic framework on carbon fabric, CoPc-P4VP = cobalt phthalocyanine poly-4-vinylpyridine). See also [65,76–78]. Abbreviations: FE, Faradaic efficiency; TOF, turnover efficiency.

The Surendranath group attached the Re(bpy)(CO)$_3$Cl catalyst to graphite using their surface conjugated pyrazine linkage [74]. The catalyst was able to reduce CO$_2$ to CO in acetonitrile with current densities greater than 50 mA/cm^2. Importantly, the **Tafel plot** showed linearity over a 0.6-V range, suggesting a change in mechanism, with higher TOF at lower overpotentials and no clear plateau at higher potentials.

In addition to understanding the surface and the strength of attachment, it is important to understand how modification of the bipyridine ligand with a surface immobilizable group affects the catalyst. In the homogeneous case, the first reduction of the Re bpy catalysts is bipyridine-ligand centered and therefore the redox potential is affected by bipyridine substituents (Figure 6) [53]. A more-negative **Hammett parameter** for the ligand is correlated with a more-negative reduction potential for the complex. However, energy matching of the bipyridine ligand and Re d_z^2 orbitals is also important, as strong electron withdrawing groups cause more positive catalyst reduction potentials, but they also encourage the charge to localize on the bpy ligand, lowering the reactivity of the Re center with CO$_2$. This understanding has led to significant optimization of the homogeneous system. When immobilized on the surface, this same approach of understanding the electronics of the Re center can lead to further improvement.
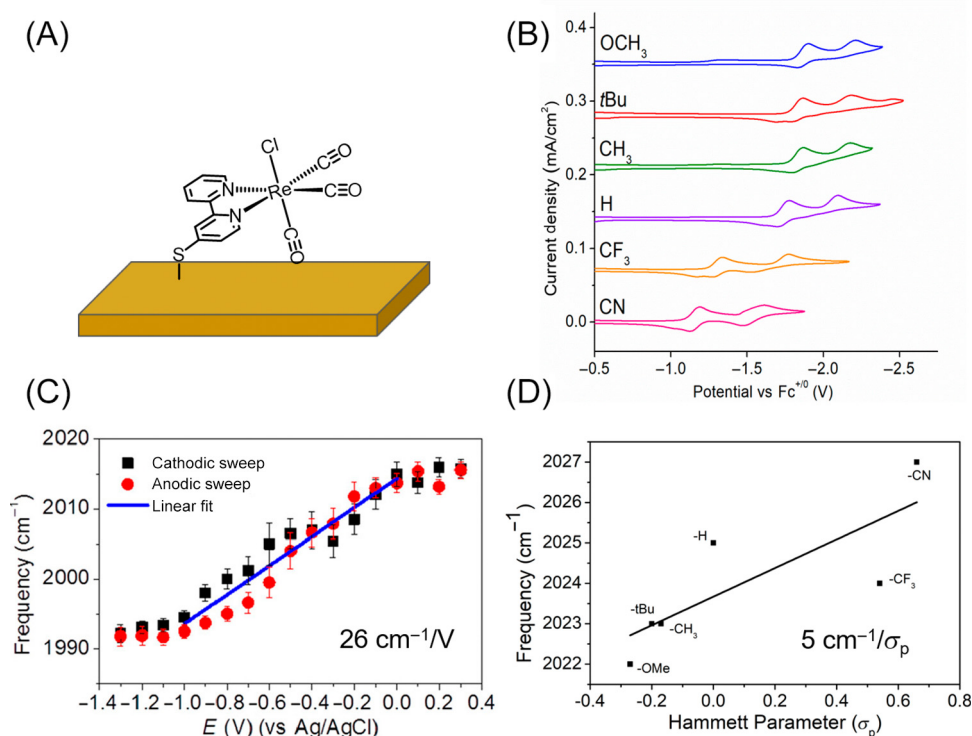
Figure 6. How Modifying the Bipyridine Ligand with a Surface Immobilizable Group Affects the Catalyst. (A) Diagram of *sum-frequency generation (SFG)* experimental setup with Re(S-bpy)(CO)3Cl attached to Au. (B) *Cyclic* voltammetry (CV) of Re bipyridine catalysts with different substituents on the ligand [53]. (C) Dependence of v*(CO) mode (cm−1)* vs applied bias. (D) Dependence of v*(CO) mode (cm−1)* vs Hammett parameter. See also [80–82].

Although the use of self-assembled monolayer approaches for Re(S-bpy)(CO)$_3$Cl attachment to a gold electrode is unable to survive the reducing potentials needed for catalysis, this system enables SFG spectroscopy to provide insight on the fundamental physical chemistry at the surface (Figure 6) [79,80]. The symmetric v(CO) band shifts linearly ~25 cm^{-1} over ~1 V of applied potential. No Faradaic current flows in this experiment. The complex is simply responding to the electric field produced by applying a bias to the electrode. This shift in the absence of current is known as the vibrational Stark–Lo Surdo effect. Dawlaty observed this phenomenon with immobilized mercaptobenzonitrile. When compared with the v(CN) energies of various organic benzonitriles, Dawlaty showed a correlation between the applied potential and the Hammett parameter. He hypothesized that polarized electrode surfaces could be used as tunable functional groups [81]. When reexamining the Re SAM work, the v(CO) shift due to the applied potential is 3–4-times larger than would be caused by Hammett substitutions. This is evidence that the field effect observed by Dawlaty can be extended to organometallic catalysts (Figure 6). The study of the effects of strong local electric fields on molecular catalysts near electrode surfaces will continue to be an important area of research.

Manipulating Reaction Pathways of Molecular Catalysts

Nature sets the standard for efficient and reversible CO_2 reduction. The metalloenzyme carbon monoxide dehydrogenase (CODH) contains a key dinuclear Ni–Fe active site that catalyzes CO_2 reduction to CO at a low overpotential ($\eta < 0.1$ V) [83]. Researchers have made attempts to mimic CODH by synthesizing catalysts with multiple reactive metal centers. Naruta and colleagues

developed co-facial iron porphyrin dimers where two triphenylporphyrins were connected by an ortho- or meta-substituted benzene [84,85]. The ortho-attached dimer exhibited the best catalytic performance in 10% H_2O/DMF with 95% FE_{CO} and a high TOF (TOF = 4300 s^{-1}) at a moderate overpotential (η = 0.66 V), which was comparable with the monometallic complex (FeTPP). The Fe–Fe separation (3.7–6.2 Å) is proposed to create a molecular pocket that can bind CO_2. The Fe–Fe arrangement is likely to enable an intramolecular 'push–pull' mechanism. When reduced, one Fe center donates an electron pair onto CO_2 as a Lewis base and the second Fe center promotes C–O bond cleavage as a Lewis acid.

Machan and colleagues reported a hydrogen bonding bimolecular assembly using two acetoamido (dac) functionalized electrocatalysts [Re(dacbpy)(CO)$_3$Cl and Mn(dacbpy)(CO)$_3$Br] [86]. Electrochemical studies showed that the redox features of the bimolecular assembly show electronic interactions between the two catalysts. CV in DMF indicated that metal–metal bond formation occurs under conditions where the respective homobimetallic analogs are not formed, which suggests that the heterobimetallic interaction reduces the redox potential. An increased catalytic current was observed for the bimolecular assembly under CO_2, which is consistent with Re–Mn cooperativity. Control experiments with methyl functionalized catalysts [Re(CH$_3$-bpy)(CO)$_3$Cl and Mn(CH$_3$-bpy)(CO)$_3$Br] showed no increased current under CO_2. Re(dacbpy)(CO)$_3$Cl is likely to operate with a similar bimolecular mechanism based on DFT calculations, molecular dynamics simulations, and IR-SEC observations [87]. This cooperative effect was also observed for a peptide functionalized Re-bpy catalyst, which was designed to promote hydrogen bonding between complexes and homodimer formation [88].

Concluding Remarks

The past decade has seen enormous increases in the activities of and decreases in the overpotential for molecular electrocatalysts for CO_2 reduction. Future studies should explore the tuning of heterodinuclear complexes to decrease overpotentials further and maintain high reaction rates (see Outstanding Questions). IR-SEC and DFT have provided richly detailed mechanistic understanding of electrocatalysts. IR-SEC is specifically useful for the Group VII metal catalysts, as their three carbonyl groups are observed in the IR range ~2100–1800 cm^{-1} and are greatly affected by the oxidation state of the metal. The use of Lewis or Brønsted acids to enhance CO selectivity is currently underutilized. Careful selection of the appropriate acids may provide similar or more leverage in manipulating the catalytic pathways than synthetic alteration of the ligands. The concept of microenvironments, which provide enzyme-like pockets for electrocatalysts with efficient mass transport of reactants and products, is particularly promising. Further development of electrocatalytic systems that reduce CO_2 at high catalytic rates and low overpotentials are crucial for the development of a sustainable chemical process to remediate anthropogenic CO_2 emissions. The key challenge facing the field of molecular electrocatalysis of CO_2 reduction is to move beyond the catalysis of two-electron processes such as CO and HCOOH formation to higher organic small-molecule liquid fuels.

References

1. Coehn, A. and Jahn, S. (1904) On the electrolytic reduction of carbon dioxide. *Ber. Dtsch. Chem. Ges.* 37, 2836–2842
2. Fischer, F. and Prziza, O. (1914) Concerning the electrolytic reduction of carbon dioxide and carbonic oxide under pressure. *Ber. Dtsch. Chem. Ges.* 47, 256–260
3. Dalle, K.E. *et al.* (2019) Electro- and solar-driven fuel synthesis with first row transition metal complexes. *Chem. Rev.* 119, 2752–2875
4. Spitler, M.T. *et al.* (2020) Practical challenges in the development of photoelectrochemical solar fuels production. *Sustain. Energy Fuels* 4, 985–995
5. Roth, S. (2019) *California has too much solar power. That might be good for ratepayers*, Los Angeles Times June 5
6. Gray, H.B. (2009) Powering the planet with solar fuel. *Nat. Chem.* 1, 7

Outstanding Questions

How does catalyst design influence the selectivity for CO_2 reduction over proton reduction?

What approaches can be used to lower the overpotential of a molecular electrocatalyst?

How do the theoretical and experimental findings in the area of electrochemical reduction of CO_2 align?

What has been learned from theoretical investigations of CO_2 reduction?

How can homogeneous catalysts bring insight into heterogeneous processes?

What electronic structural characteristics contribute to efficient electrochemical reduction of CO_2 by molecular catalysts?

7. Crabtree, R.H. (2020) Alternate strategies for solar fuels from carbon dioxide. *ACS Energy Lett.* 5, 2505–2507
8. Jiang, C. *et al.* (2019) A look at periodic trends in d-block molecular electrocatalysts for CO_2 reduction. *Dalton Trans.* 48, 9454–9468
9. Takeda, H. *et al.* (2017) Electrons, photons, protons and earth-abundant metal complexes for molecular catalysis of CO_2 reduction. *ACS Catal.* 7, 70–88
10. Meshitsuka, S. *et al.* (1974) Electrocatalysis by metal phthalocyanines in the reduction of carbon dioxide. *J. Chem. Soc. Chem. Commun.* 5, 158–159
11. Kazuya, H. *et al.* (1977) Electrocatalytic behavior of tetra-sulfonated metal phthalocyanines in the reduction of carbon dioxide. *Chem. Lett.* 6, 1137–1140
12. Fisher, B.J. and Eisenberg, R. (1980) Electrocatalytic reduction of carbon dioxide by using macrocycles of nickel and cobalt. *J. Am. Chem. Soc.* 102, 7361–7363
13. Beley, M. *et al.* (1984) Nickel(II)-cyclam: an extremely selective electrocatalyst for reduction of carbon dioxide in water. *J. Chem. Soc. Chem. Commun.* 19, 1315–1316
14. Slater, S. and Wagenknecht, J.H. (1984) Electrochemical reduction of carbon dioxide catalyzed by Rh(diphos)$_2$Cl. *J. Am. Chem. Soc.* 106, 5367–5368
15. Hawecker, J. *et al.* (1984) Electrocatalytic reduction of carbon dioxide mediated by Re(bipy)(CO)$_3$Cl (bipy = 2,2'-bipyridine). *J. Chem. Soc. Chem. Commun.* 6, 328–330
16. Costentin, C. and Savéant, J-M. (2014) Multielectron, multistep molecular catalysis of electrochemical reactions: benchmarking of homogeneous catalysts. *ChemElectroChem* 1, 1226–1236
17. Loewen, N.D. *et al.* (2017) Renewable formate from C–H bond formation with CO_2: using iron carbonyl clusters as electrocatalysts. *Acc. Chem. Res.* 50, 2362–2370
18. Cluff, D.B. *et al.* (2019) Electrocatalytic reduction of CO_2 into formate with glassy carbon modified by [Fe$_4$N(CO)$_{11}$(PPh$_2$Ph-linker)]$^-$. *Organometallics* 38, 1230–1235
19. Yang, J.Y. *et al.* (2020) Reducing CO_2 to HCO$_2^-$ at mild potentials: lessons from formate dehydrogenase. *J. Am. Chem. Soc.* 142, 19438–19445
20. Cunningham, D.W. and Yang, J.Y. (2020) Kinetic and mechanistic analysis of a synthetic reversible CO_2/HCO$_2^-$ electrocatalyst. *Chem. Commun.* 56, 12965–12968
21. Zhang, S. *et al.* (2020) CO_2 reduction: from homogeneous to heterogeneous electrocatalysis. *Acc. Chem. Res.* 53, 255–264
22. Nakata, K. *et al.* (2014) High-yield electrochemical production of formaldehyde from CO_2 and seawater. *Angew. Chem. Int. Ed.* 53, 871–874
23. Boutin, E. *et al.* (2019) Aqueous electrochemical reduction of carbon dioxide and carbon monoxide into methanol with cobalt phthalocyanine. *Angew. Chem. Int. Ed.* 558, 16172–16176
24. Liu, Y. *et al.* (2019) Steering CO_2 electroreduction toward ethanol production by a surface-bound Ru polypyridyl carbene catalyst on N-doped porous carbon. *Proc. Natl. Acad. Sci. U. S. A.* 116, 26353
25. Keith, J.A. *et al.* (2013) Elucidation of the selectivity of proton-dependent electrocatalytic CO_2 reduction by *fac*-Re(bpy)(CO)$_3$Cl. *J. Am. Chem. Soc.* 135, 15823–15829
26. Riplinger, C. *et al.* (2014) Mechanistic contrasts between manganese and rhenium bipyridine electrocatalysts for the reduction of carbon dioxide. *J. Am. Chem. Soc.* 136, 16285–16298
27. Sampson, M.D. *et al.* (2013) Direct observation of the reduction of carbon dioxide by rhenium bipyridine catalysts. *Energy Environ. Sci.* 6, 3748–3755
28. Grice, K.A. *et al.* (2013) Carbon monoxide release catalysed by electron transfer: electrochemical and spectroscopic investigations of [Re(bpy-R)(CO)$_4$](OTf) complexes relevant to CO_2 reduction. *Dalton Trans.* 42, 8498–8503
29. Benson, E.E. *et al.* (2013) The electronic states of rhenium bipyridyl electrocatalysts for CO_2 reduction as revealed by X-ray absorption spectroscopy and computational quantum chemistry. *Angew. Chem. Int. Ed.* 52, 4841–4844
30. Benson, E.E. *et al.* (2013) Structural and spectroscopic studies of reduced [Re(bpy-R)(CO)$_3$]$^{-1}$ species relevant to CO_2 reduction. *Polyhedron* 58, 229–234
31. Smieja, J.M. and Kubiak, C.P. (2010) Re(bipy-*t*Bu)(CO)$_3$Cl-improved catalytic activity for reduction of carbon dioxide:

32. Benson, E.E. and Kubiak, C.P. (2012) Structural investigations into the deactivation pathway of the CO_2 reduction electrocatalyst Re (bpy)(CO)$_3$Cl. *Chem. Commun.* 48, 7374–7376
33. Kallane, S.I. and van Gastel, M. (2016) Raman spectroscopy as a method to investigate catalytic intermediates: CO_2 reducing [Re(Cl)(bpy-R)(CO)$_3$] catalyst. *J. Phys. Chem. A* 120, 7465–7474
34. Sullivan, B.P. *et al.* (1985) One- and two- electron pathways in the electrocatalytic reduction of CO_2 by *fac*-Re(bpy)(CO)$_3$Cl (bpy = 2,2'-bipyridine). *J. Chem. Soc. Chem. Commun.* 20, 1414–1416
35. Johnson, F.P.A.G. *et al.* (1996) Electrocatalytic reduction of CO_2 using the complexes [Re(bpy)(CO)$_3$L]^n (n = +1, L = P(OEt)$_3$, CH$_3$CN; n = 0, L = Cl$^-$, Otf$^-$; bpy = 2,2'-bipyridine; Otf$^-$ = CF$_3$SO$_3$) as catalyst precursors: infrared spectroelectrochemical investigation. *Organometallics* 15, 3374–3387
36. Agarwal, J. *et al.* (2012) Mechanisms for CO production from CO_2 using reduced rhenium tricarbonyl catalysts. *J. Am. Chem. Soc.* 134, 5180–5186
37. Bourrez, M. *et al.* (2011) [Mn(bipyridyl)CO$_3$Br]: an abundant metal carbonyl complex as efficient electrocatalyst for CO_2 reduction. *Angew. Chem. Int. Ed.* 50, 9903–9906
38. Ngo, K.T. *et al.* (2017) Turning on the protonation-first pathway for electrocatalytic CO_2 reduction by manganese bipyridyl tricarbonyl complexes. *J. Am. Chem. Soc.* 139, 2604–2618
39. Walsh, J.J. *et al.* (2019) Water-soluble manganese complex for selective electrocatalytic CO_2 reduction to CO. *Organometallics* 38, 1224–1229
40. Grills, D.C. *et al.* (2018) Mechanistic aspects of CO_2 reduction catalysis with manganese-based molecular catalysts. *Coord. Chem. Rev.* 374, 173–217
41. Cheung, P.L. *et al.* (2016) Photocatalytic reduction of carbon dioxide to CO and HCO$_2$H using *fac*-Mn(CN)(bpy)(CO)$_3$. *Inorg. Chem.* 55, 3192–3198
42. Rønne, M.H. *et al.* (2020) Ligand-controlled product selectivity in electrochemical carbon dioxide reduction using manganese bipyridine catalysts. *J. Am. Chem. Soc.* 142, 4265–4275
43. Machan, C.W. *et al.* (2015) Electrocatalytic reduction of carbon dioxide by Mn(CN)(2,2'-bipyridine)(CO)$_3$: CN coordination alters mechanism. *Inorg. Chem.* 54, 8849–8856
44. Tignor, S.E. *et al.* (2019) Manganese-based catalysts with varying ligand substituents for the electrochemical reduction of CO_2 to CO. *Organometallics* 38, 1292–1299
45. Agnew, D.W. *et al.* (2016) Electrochemical properties and CO_2-reduction ability of *m*-terphenyl isocyanide supported manganese tricarbonyl complexes. *Inorg. Chem.* 55, 12400–12408
46. Compain, J.D. *et al.* (2014) Manganese carbonyl terpyridyl complexes: their synthesis, characterization and potential application as CO-release molecules. *Chem. Commun.* 50, 2539–2542
47. Grills, D.C. *et al.* (2014) Mechanism of the formation of a Mn-based CO_2 reduction catalyst revealed by pulse radiolysis with time-resolved infrared detection. *J. Am. Chem. Soc.* 136, 5563–5566
48. Smieja, J.M. *et al.* (2013) Manganese as a substitute for rhenium in CO_2 reduction catalysts: the importance of acids. *Inorg. Chem.* 52, 2484–2491
49. Takeda, H.K. *et al.* (2014) Photocatalytic CO_2 reduction using a Mn complex as a catalyst. *Chem. Commun.* 50, 1491–1493
50. Sampson, M.D. and Kubiak, C.P. (2016) Manganese electro-catalysts with bulky bipyridine ligands: utilizing Lewis acids to promote carbon dioxide reduction at low overpotentials. *J. Am. Chem. Soc.* 138, 1386–1393
51. Sampson, M.D. *et al.* (2014) Manganese catalysts with bulky bipyridine ligands for the electrocatalytic reduction of carbon dioxide: eliminating dimerization and altering catalysis. *J. Am. Chem. Soc.* 136, 5460–5471
52. Rountree, E.S. *et al.* (2014) Evaluation of homogeneous electrocatalysts by cyclic voltammetry. *Inorg. Chem.* 53, 9983–10002
53. Clark, M.L. *et al.* (2018) Kinetic and mechanistic effects of bipyridine (bpy) substituent, labile ligand, and Brønsted acid on electrocatalytic CO_2 reduction by Re(bpy) complexes. *ACS Catal.* 8, 2021–2029

54. Riplinger, C. and Carter, E.A. (2015) Influence of weak Brønsted acids on electrocatalytic CO2 reduction by manganese and rhenium bipyridine catalysts. *ACS Catal.* 5, 900–908

55. Wang, X. *et al.* (2019) A rational design of manganese electrocatalysts for Lewis acid-assisted carbon dioxide reduction. *Phys. Chem. Chem. Phys.* 21, 8849–8855

56. Zhanaidarova, A. *et al.* (2017) Chelated [Zn(cyclam)]$^{2+}$ Lewis acid improves the reactivity of the electrochemical reduction of CO_2 by Mn catalysts with bulky bipyridine ligands. *Dalton Trans.* 46, 12413–12416

57. Clark, M.L. *et al.* (2014) Electrocatalytic CO_2 reduction by M(bpy-R) (CO)$_4$ (M = Mo, W; R = H, *t*Bu) complexes. Electrochemical, spectroscopic, and computational studies and comparison with Group 7 catalysts. *Chem. Sci.* 5, 1894–1900

58. Tory, J. *et al.* (2015) [M(CO)$_4$(2,2'-bipyridine)] (M=Cr, Mo, W) complexes as efficient catalysts for electrochemical reduction of CO_2 at a gold electrode. *ChemElectroChem* 2, 213–217

59. Neri, G. *et al.* (2017) The role of electrode-catalyst interactions in enabling efficient CO_2 reduction with Mo(bpy)(CO)$_4$ as revealed by vibrational sum-frequency generation spectroscopy. *J. Am. Chem. Soc.* 139, 13791–13797

60. An, L. and Chen, R. (2016) Direct formate fuel cells: a review. *J. Power Sources* 320, 127–139

61. Chen, X. *et al.* (2020) Understanding the enhanced catalytic CO_2 reduction upon adhering cobalt porphyrin to carbon nanotubes and the inverse loading effect. *Organometallics* 39, 1634–1641

62. Grammatico, D. *et al.* (2020) Immobilization of a molecular Re complex on MOF-derived hierarchical porous carbon for CO_2 electroreduction in water/ionic liquid electrolyte. *ChemSusChem* 13, 6418–6425

63. Sun, L. *et al.* (2020) Electrocatalytic reduction of carbon dioxide: opportunities with heterogeneous molecular catalysts. *Energy Environ. Sci.* 13, 374–403

64. Zhu, M. *et al.* (2019) Cobalt phthalocyanine coordinated to pyridine-functionalized carbon nanotubes with enhanced CO_2 electroreduction. *Appl. Catal. B Environ.* 251, 112–118

65. Sato, S. *et al.* (2018) Low-energy electrocatalytic CO_2 reduction in water over Mn-complex catalyst electrode aided by a nanocarbon support and K$^+$ cations. *ACS Catal.* 8, 4452–4458

66. Sato, S. *et al.* (2020) Aqueous electrocatalytic CO_2 reduction using metal complexes dispersed in polymer ion gels. *Chem. Commun.* 56, 4440–4443

67. Zhu, M. *et al.* (2019) Covalently grafting cobalt porphyrin onto carbon nanotubes for efficient CO_2 electroreduction. *Angew. Chem. Int. Ed.* 58, 6595–6599

68. Zhu, M. *et al.* (2019) Electronic tuning of cobalt porphyrins immobilized on nitrogen-doped graphene for CO_2 reduction. *ACS Appl. Energy Mater.* 2, 2435–2440

69. Orchanian, N.M. *et al.* (2019) Immobilized molecular wires on carbon-cloth electrodes facilitate CO_2 electrolysis. *ACS Catal.* 9, 9393–9397

70. O'Toole, T.R. *et al.* (1985) Electrocatalytic reduction of CO_2 at a chemically modified electrode. *J. Chem. Soc. Chem. Commun.* 20, 1416–1417

71. Cabrera, C.R. and Abruña, H.D. (1986) Electrocatalysis of CO_2 reduction at surface modified metallic and semiconducting electrodes. *J. Electroanal. Chem. Interfacial Electrochem.* 209, 101–107

72. Zhanaidarova, A. *et al.* (2019) Selective reduction of CO_2 to CO by a molecular Re(ethynyl-bpy)(CO)$_3$Cl catalyst and attachment to carbon electrode surfaces. *Organometallics* 38, 1204–1207

73. Orchanian, N.M. *et al.* (2019) Surface-immobilized conjugated polymers incorporating rhenium bipyridine motifs for electrocatalytic and photocatalytic CO_2 reduction. *ACS Appl. Energy Mater.* 2, 110–123

74. Oh, S. *et al.* (2016) Graphite-conjugated rhenium catalysts for carbon dioxide reduction. *J. Am. Chem. Soc.* 138, 1820–1823

75. Zhanaidarova, A. *et al.* (2019) Re(*t*Bu-bpy)(CO)$_3$Cl supported on multi-walled carbon nanotubes selectively reduces CO_2 in water. *J. Am. Chem. Soc.* 141, 17270–17277

76. Kramer, W.W. and McCrory, C.C.L. (2016) Polymer coordination promotes selective CO_2 reduction by cobalt phthalocyanine. *Chem. Sci.* 7, 2506–2515

77. Zhang, X. *et al.* (2017) Highly selective and active CO_2 reduction electrocatalysts based on cobalt phthalocyanine/carbon nanotube hybrid structures. *Nat. Commun.* 8, 14675

78. Lin, S. *et al.* (2015) Covalent organic frameworks comprising cobalt porphyrins for catalytic CO_2 reduction in water. *Science* 349, 1208

79. Clark, M.L. *et al.* (2018) CO_2 reduction catalysts on gold electrode surfaces influenced by large electric fields. *J. Am. Chem. Soc.* 140, 17643–17655

80. Gardner, A.M. *et al.* (2019) Vibrational sum-frequency generation spectroscopy of electrode surfaces: studying the mechanisms of sustainable fuel generation and utilisation. *Phys. Chem. Chem. Phys.* 21, 12067–12086

81. Sarkar, S. *et al.* (2019) Electrodes as polarizing functional groups: correlation between Hammett parameters and electrochemical polarization. *J. Phys. Chem. C* 123, 4926–4937

82. Ge, A. *et al.* (2019) Heterogenized molecular catalysts: vibrational sum-frequency spectroscopic, electrochemical, and theoretical investigations. *Acc. Chem. Res.* 52, 1289–1300

83. Shin, W. *et al.* (2003) Highly selective electrocatalytic conversion of CO_2 to CO at -0.57 V (NHE) by carbon monoxide dehydrogenase from *Moorella thermoacetica*. *J. Am. Chem. Soc.* 125, 14688–14689

84. Mohamed, E.A. *et al.* (2015) Efficient electrocatalytic CO_2 reduction with a molecular cofacial iron porphyrin dimer. *Chem. Commun.* 51, 16900–16903

85. Zahran, Z.N. *et al.* (2016) Bio-inspired cofacial Fe porphyrin dimers for efficient electrocatalytic CO_2 to CO conversion: overpotential tuning by substituents at the porphyrin rings. *Sci. Rep.* 6, 24533

86. Machan, C.W. and Kubiak, C.P. (2016) Interrogating heterobimetallic co-catalytic responses for the electrocatalytic reduction of CO_2 using supramolecular assembly. *Dalton Trans.* 45, 15942–15950

87. Machan, C.W. *et al.* (2016) Improving the efficiency and activity of electrocatalysts for the reduction of CO_2 through supramolecular assembly with amino acid-modified ligands. *J. Am. Chem. Soc.* 138, 8184–8193

88. Chabolla, S.A. *et al.* (2017) Bio-inspired CO_2 reduction by a rhenium tricarbonyl bipyridine-based catalyst appended to amino acids and peptidic platforms: incorporating proton relays and hydrogen-bonding functional groups. *Faraday Discuss.* 198, 279–300